



# Nobel metal free, oxidant free, solvent free catalytic transformation of alcohol to aldehyde over ZnO-CeO<sub>2</sub> mixed oxide catalyst



Nagasuresh Enjamuri<sup>a</sup>, Shahid Hassan<sup>a</sup>, Aline Auroux<sup>b,\*</sup>, Jai Krishna Pandey<sup>c</sup>, Biswajit Chowdhury<sup>a,\*</sup>

<sup>a</sup> Department of Applied Chemistry, Indian School of Mines, Dhanbad, India

<sup>b</sup> Institut de Recherches sur la Catalyse et l'Environnement de Lyon, UMR 5256, CNRS-UCB Lyon 1, 2 av. Albert Einstein, 69626 Villeurbanne Cedex, France

<sup>c</sup> Central Institute of Mining and Fuel research (CIMFR) Dhanbad, India

## ARTICLE INFO

### Article history:

Received 19 February 2016

Received in revised form 23 April 2016

Accepted 3 May 2016

Available online 11 May 2016

### Keywords:

Dehydrogenation

Benzyl alcohol

Propane

Zinc

Ceria

Toluene

## ABSTRACT

The catalytic transformation of alcohols to aldehydes under oxidant-free condition has drawn significant attention from the perspective of green chemistry. In this work, we designed noble metal free ZnO-CeO<sub>2</sub> mixed oxide catalyst in four different ratios and tested for vapor phase benzyl alcohol dehydrogenation reaction as a model reaction under oxidant free condition. The ZnO-CeO<sub>2</sub> mixed oxide catalyst having ratio Zn/Ce = 30/70 composition showed highest selectivity towards formation of benzaldehyde. Interestingly in addition to benzaldehyde, toluene was formed in the reaction due to hydrogenolysis of benzyl alcohol. The lowest Ce<sup>3+</sup>/Ce<sup>4+</sup> ratio was observed from the XPS analysis of Ce(3d) core electron for the catalyst having Zn/Ce = 30/70 composition compared to others. CO<sub>2</sub>-TPD results proved that mostly the medium strength basic sites were responsible for hydrogen abstraction from benzyl alcohol producing benzaldehyde. H<sub>2</sub>-TPR results showed that ZnO-CeO<sub>2</sub> catalyst (Zn/Ce = 30:70) had lowest reduction temperature which is in the 673 K to 573 K temperature range. The amount of toluene was higher for the ZnO-CeO<sub>2</sub> catalyst having Zn/Ce = 40:60 ratio which had less basic sites and higher fraction of Ce<sup>3+</sup> ion. The ZnO-CeO<sub>2</sub> catalyst (Zn/Ce = 30:70) did not deactivate for a reaction time up to 2 h. While successive regenerations of the catalyst, toluene selectivity were increased. This may be due to the reduction of Ce<sup>4+</sup> to Ce<sup>3+</sup> by adsorbed hydrogen species. Also the ZnO-CeO<sub>2</sub> catalyst (Zn/Ce = 30/70) showed activity for the formation of ethanal, propanal, butanal and octanal along with corresponding alkanes from ethanol, 1-propanol, 1-butanol and 1-octanol in oxidant free condition demonstrating the in-situ generation of hydrogen. The micro kinetic analysis showed that there is no external and internal mass transfer limitation in the present case.

© 2016 Elsevier B.V. All rights reserved.

## 1. Introduction

In the catalytic thermal decomposition of alcohols, it is commonly known that dehydrogenation reaction proceeds on metal surfaces [1]. A previous study shows that decomposition of alcohols takes place on reduced copper powders [2]. During dehydrogenation process hydrogen was chemisorbed on the metal surface [3]. Recent reports reveals that Ag and Cu nanoparticles supported on TiO<sub>2</sub> and hydrotalcite materials were effectually catalyze the dehydrogenation of various alcohols [4–6], particularly benzyl alcohol to benzaldehyde is one of the most important reaction because of

its wider applications [7]. Traditionally, benzaldehyde is produced through stoichiometric oxidation of manganese and chromium salts or by the hydrolysis of benzyl chloride and the oxidation of toluene in industrial processes [8]. Although there are many methods for the oxidation of benzyl alcohol to benzaldehyde by using molecular oxygen catalyzed by Au nanoparticles supported on CeO<sub>2</sub>, TiO<sub>2</sub>, MnO<sub>2</sub>, hydrotalcite and bimetallic Au-Pd/TiO<sub>2</sub> [9,10]. Alternative designs for the development of promising oxidant-free methodology are particularly interesting due to inhibition towards over oxidation of the substrate to form carboxylic acid [11]. In this scenario the ceria based catalysts have drawn attention recently, due to Ce<sup>3+</sup>/Ce<sup>4+</sup> redox couple it alters the ionicity and covalent nature of the metal-oxygen bond by creation of the acidic/basic sites on its surface [12]. An amphoteric nature of ceria are widely used either as a support or active component in versatile reactions e.g. water-gas shift reaction [13], CO oxidation [14], allylic oxidation

\* Corresponding authors.

E-mail addresses: [aline.auroux@ircelyon.univ-lyon1.fr](mailto:aline.auroux@ircelyon.univ-lyon1.fr) (A. Auroux), [biswajit.chem2003@yahoo.com](mailto:biswajit.chem2003@yahoo.com) (B. Chowdhury).

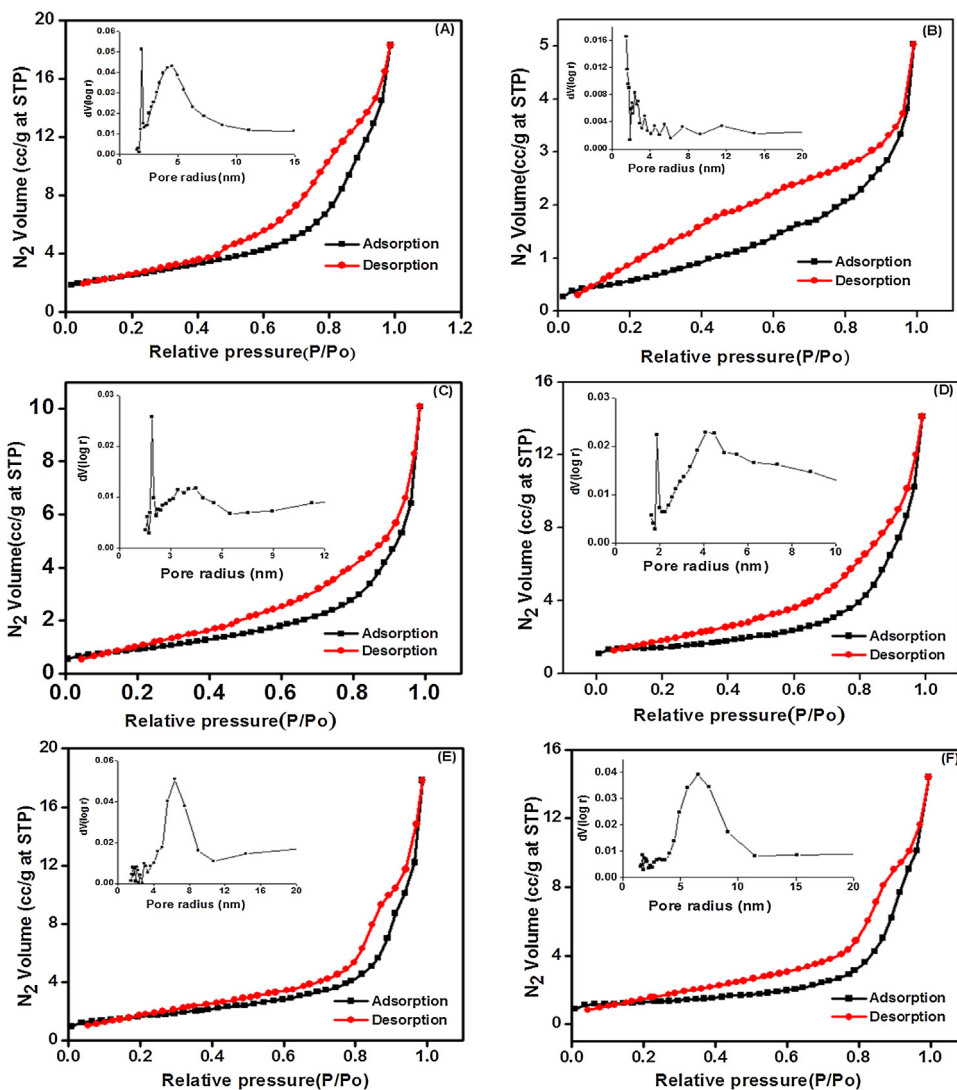


**Fig. 1.** BET S.A of (A)  $\text{CeO}_2$ , (B)  $\text{ZnO}$ , (C)  $\text{ZnO}-\text{CeO}_2$  ( $\text{Zn}/\text{Ce} = 20:80$ ), (D)  $\text{ZnO}-\text{CeO}_2$  ( $\text{Zn}/\text{Ce} = 30:70$ ), (E)  $\text{ZnO}-\text{CeO}_2$  ( $\text{Zn}/\text{Ce} = 40:60$ ) & (F)  $\text{ZnO}-\text{CeO}_2$  ( $\text{Zn}/\text{Ce} = 50:50$ ) inset shows the pore size distribution of the respective catalysts.

**Table 1**  
Summary of surface area and porosity results of Zinc-ceria mixed oxide catalysts.

Catalyst	Surface Area ( $\text{m}^2/\text{g}$ )	Total pore volume (cc/g)	Av. Pore diameter (nm)
$\text{CeO}_2$	8.84	0.029	3.8
$\text{ZnO}-\text{CeO}_2$ ( $\text{Zn}/\text{Ce} = 20:80$ )	3.39	0.016	3.7
$\text{ZnO}-\text{CeO}_2$ ( $\text{Zn}/\text{Ce} = 30:70$ )	4.68	0.021	3.8
$\text{ZnO}-\text{CeO}_2$ ( $\text{Zn}/\text{Ce} = 40:60$ )	5.84	0.027	12.8
$\text{ZnO}-\text{CeO}_2$ ( $\text{Zn}/\text{Ce} = 50:50$ )	4.15	0.022	11.2
$\text{ZnO}$	2.38	0.007	3.0

[15], alcohol oxidation [29], knoevenagel condensation [16] etc.  $\text{CeO}_2$  has face-centered cubic crystal structure, into which various cation dopants can be introduced in order to increase the physico-chemical properties of ceria [17–19]. the modification of  $\text{CeO}_2$  with  $\text{Zn}^{2+}$  ions leads to creation of oxygen ion vacancy around the  $\text{Zn}^{2+}$  ion in the  $\text{CeO}_2$  based mixed oxide catalysts.

H. Imai et al. [20] have reported little activity towards methanol dehydrogenation over zinc and zinc alloy catalyst system. Zinc supported on ceria catalyst has been reported by yongjun He et al. [21] for the oxidative coupling of methane with carbon dioxide. In another study B. G. Mishra et al. [22] reported the  $\text{CeO}_2-\text{ZnO}$  composite oxide for cyclohexanol dehydrogenation reaction.

In this work, it is hypothesized that substitution of lower valent  $\text{Zn}^{2+}$  ion to the ceria may increase the ionicity of the M-O-M' bond leads to form acidic/basic properties which can abstract hydrogen from the alcohols. The four different Zinc-ceria mixed oxide catalysts with different  $\text{Zn}/\text{Ce}$  ratio 20:80; 30:70; 40:60; 50:50 were synthesized and characterized by XRD,  $\text{N}_2$ -Physisorption, UV-vis, XPS,  $\text{CO}_2$ -TPD and  $\text{H}_2$ -TPR techniques. The several reaction parameters like reaction temperature, pretreatment temperature, and pretreatment time were varied for benzyl alcohol reaction to find an optimum catalytic activity. The catalytic activity was evaluated for the benzyl alcohol, Ethanol, 1-propanol, 1-butanol and 1-octanol dehydrogenation reaction by using fixed-bed catalytic reactor in an inert atmosphere condition. Interestingly toluene was formed

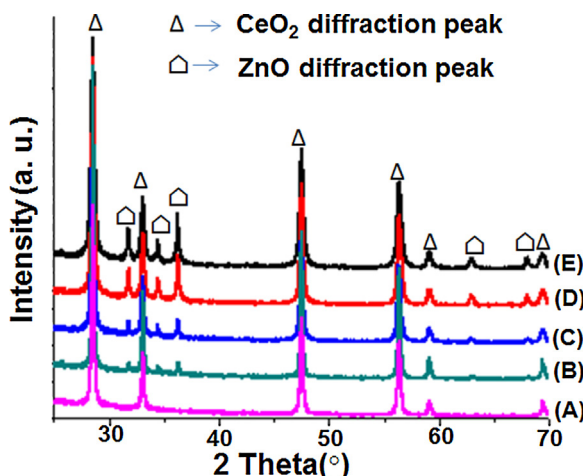


**Fig. 2.** X-ray diffraction patterns of (A)  $\text{CeO}_2$ , (B)  $\text{ZnO}-\text{CeO}_2$  ( $\text{Zn}/\text{Ce} = 20/80$ ), (C)  $\text{ZnO}-\text{CeO}_2$  ( $\text{Zn}/\text{Ce} = 30/70$ ), (D)  $\text{ZnO}-\text{CeO}_2$  ( $\text{Zn}/\text{Ce} = 40/60$ ) & (E)  $\text{ZnO}-\text{CeO}_2$  ( $\text{Zn}/\text{Ce} = 50/50$ ).

along with the benzaldehyde in the reaction of benzyl alcohol whereas ethane, propane, butane and octane were formed in the dehydrogenation of ethanol, 1-propanol, 1-butanol and 1-octanol. The micro-kinetic analysis was done for the reaction of benzyl alcohol. The special surface property of zinc-ceria mixed oxide catalyst has been discussed in the following section.

## 2. Experimental

### 2.1. Catalyst preparation

Zinc-ceria mixed oxide was prepared by the non-hydrothermal sol-gel method as described earlier [16]. In this procedure the solution of 15.2 g (0.07 mol)  $\text{Ce}(\text{NO}_3)_3 \cdot 6\text{H}_2\text{O}$  (Aldrich) was added to 14.9 g (0.2 mol) triethanolamine (Acros)/water mixture under stirring condition at room temperature. After complete addition of cerium nitrate solution, 4.5 g (0.03 mol) zinc nitrate solution was added to it with a constant stirring. This total content was stirred for 10 min and after that 7.3 g (0.1 mol) tetraethyl ammonium hydroxide (Merck, Germany) was added drop wise in the resulting solution. The mixture was kept in constant stirring condition at room temperature which forms a gel of composition; triethanolamine:  $\text{Ce}(\text{NO}_3)_3 \cdot 6\text{H}_2\text{O}$ :  $\text{H}_2\text{O}$ :  $\text{Zn}(\text{NO}_3)_2 \cdot 6\text{H}_2\text{O}$ : tetraethyl ammonium hydroxide 0.2: x: 1.1: (0.1-x): 0.1 molar ratio (where x = 0.08–0.05). The gel material was dried at 383 K for 24 h and it was calcined at 973 K for 10 h in a furnace (Thermocraft; USA) with temperature ramp of 1 °C/min.

### 2.2. Catalyst characterization

#### 2.2.1. BET surface area and porosity measurements

The BET surface area and pore size analysis of the samples were measured at liquid nitrogen temperature (77 K) with a Nova 3200e instrument (Quantachrome; USA). Before the measurement of surface area, the pretreatment of the samples was done at 473 K for 5 h under high vacuum condition. The surface area was calculated by the Brunauer–Emmett–Teller (BET) equation. The pore size distributions were calculated using the BJH method.

#### 2.2.2. X-ray diffraction (XRD)

XRD patterns and catalyst crystalline phases were identified at ambient temperature in an X-ray diffractometer (Rigaku, Ultima IV) using  $\text{Cu K}\alpha$  radiation as the X-ray source (40 kV, 20 mA), wavelength ( $\lambda$ ) =  $1.54056\text{\AA}^0$ ). The XRD results were analyzed quantitatively using X'pert software. The average crystallite

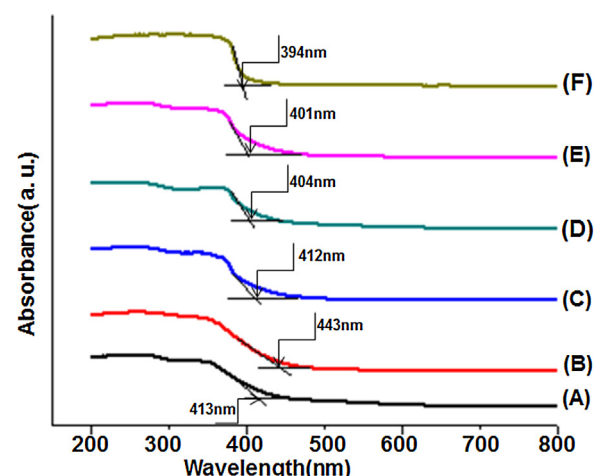


**Fig. 3.** UV-vis spectra of (A)  $\text{CeO}_2$ , (B)  $\text{ZnO}-\text{CeO}_2$  ( $\text{Zn}/\text{Ce} = 20/80$ ), (C)  $\text{ZnO}-\text{CeO}_2$  ( $\text{Zn}/\text{Ce} = 30/70$ ), (D)  $\text{ZnO}-\text{CeO}_2$  ( $\text{Zn}/\text{Ce} = 40/60$ ), (E)  $\text{ZnO}-\text{CeO}_2$  ( $\text{Zn}/\text{Ce} = 50/50$ ) & (F)  $\text{ZnO}$  catalysts.

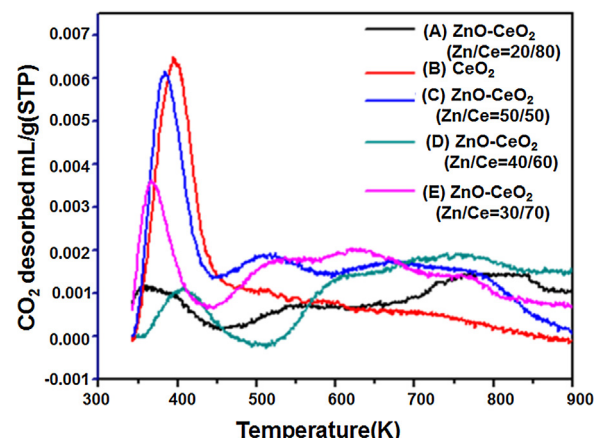


**Fig. 4.**  $\text{CO}_2$ -TPD traces of the catalysts (A)  $\text{ZnO}-\text{CeO}_2$  ( $\text{Zn}/\text{Ce} = 20/80$ ), (B)  $\text{CeO}_2$ , (C)  $\text{ZnO}-\text{CeO}_2$  ( $\text{Zn}/\text{Ce} = 50/50$ ), (D)  $\text{ZnO}-\text{CeO}_2$  ( $\text{Zn}/\text{Ce} = 40/60$ ) & (E)  $\text{ZnO}-\text{CeO}_2$  ( $\text{Zn}/\text{Ce} = 30/70$ ).

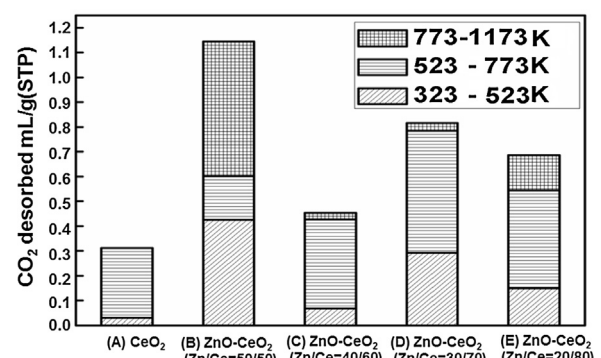


**Fig. 5.** Quantitative  $\text{CO}_2$  desorption profile of the catalysts (A)  $\text{CeO}_2$ , (B)  $\text{ZnO}-\text{CeO}_2$  ( $\text{Zn}/\text{Ce} = 50/50$ ), (C)  $\text{ZnO}-\text{CeO}_2$  ( $\text{Zn}/\text{Ce} = 40/60$ ), (D)  $\text{ZnO}-\text{CeO}_2$  ( $\text{Zn}/\text{Ce} = 30/70$ ), (E)  $\text{ZnO}-\text{CeO}_2$  ( $\text{Zn}/\text{Ce} = 20/80$ ).

sizes were estimated by considering the most intense  $\text{CeO}_2$  diffraction peak (111) located at  $2\theta = 28.55^\circ$  through Scherrer's formula  $D = 0.94K/\beta\cos\theta$  where D, K,  $\beta$ , and  $\theta$  are the average crystallite size, X-ray wavelength, peak width and Bragg's angle respectively.

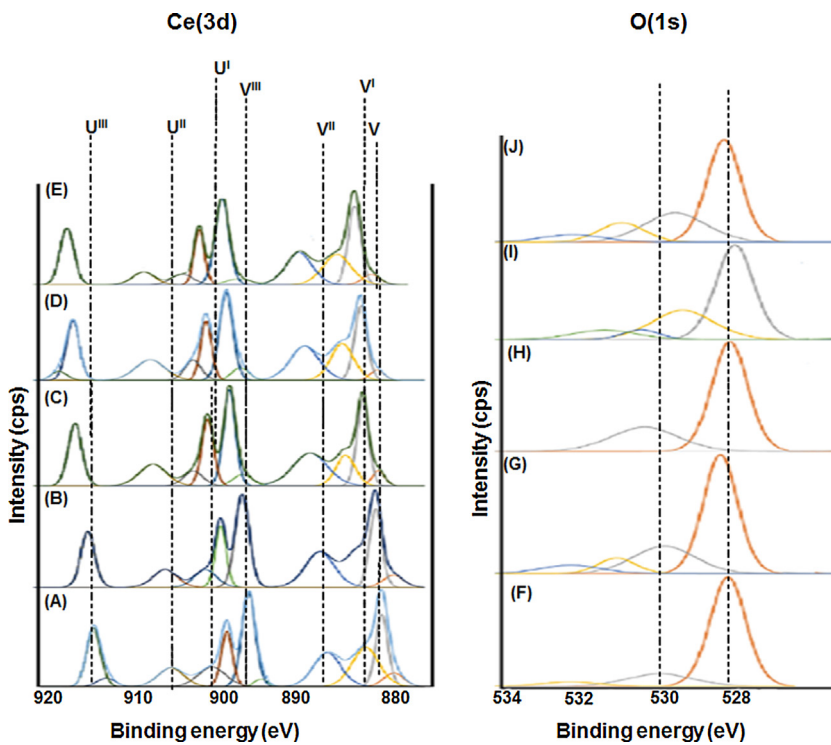


**Fig. 6.** Ce(3d) core level XPS spectra of (A)  $\text{CeO}_2$ , (B) ZnO-CeO<sub>2</sub> (Zn/Ce = 20/80), (C) ZnO-CeO<sub>2</sub> (Zn/Ce = 30:70), (D) ZnO-CeO<sub>2</sub> (Zn/Ce = 40/60) & (E) ZnO-CeO<sub>2</sub> (Zn/Ce = 50/50) catalyst O(1s) core level XPS spectra (F)  $\text{CeO}_2$ , (G) ZnO-CeO<sub>2</sub> (Zn/Ce = 20/80), (H) ZnO-CeO<sub>2</sub> (Zn/Ce = 30:70), (I) ZnO-CeO<sub>2</sub> (Zn/Ce = 40/60) & (J) ZnO-CeO<sub>2</sub> (Zn/Ce = 50/50).

**Table 2**

Quantitative analysis of X-ray diffraction patterns of Zinc-ceria mixed oxide catalysts.

Catalyst	Phase	d spacing (nm)	Crystallize size <sup>a</sup> (nm)	Cell parameter <sup>b</sup> (nm)
$\text{CeO}_2$	Cerianite	0.312375	89.18	0.5410335
ZnO- $\text{CeO}_2$ (Zn/Ce = 20:80)	Cerianite	0.312268	50.96	0.5408481
ZnO- $\text{CeO}_2$ (Zn/Ce = 30:70)	Cerianite	0.310998	14.86	0.5386485
ZnO- $\text{CeO}_2$ (Zn/Ce = 40:60)	Cerianite	0.309166	14.87	0.5354755
ZnO- $\text{CeO}_2$ (Zn/Ce = 50:50)	Cerianite	0.311767	14.86	0.5399804

<sup>a</sup> Estimated by Scherrer equation.

<sup>b</sup> by using the equation  $\frac{1}{d^2} = \frac{h^2+k^2+l^2}{a}$ .

**Table 3**

Quantitative analysis of Ce (3d) XPS spectra of Zinc-ceria mixed oxides.

Catalyst	Ce [III]	Ce [IV]	Ce[III]/Ce[IV]	Ce <sup>+3</sup> fraction	%Ce <sup>+3</sup>
$\text{CeO}_2$	22.44	29.40	0.76	0.43	43.28
ZnO- $\text{CeO}_2$ (Zn/Ce = 20:80)	19.92	30.86	0.65	0.39	39.22
ZnO- $\text{CeO}_2$ (Zn/Ce = 30:70)	12.70	29.80	0.43	0.29	29.88
ZnO- $\text{CeO}_2$ (Zn/Ce = 40:60)	17.25	29.14	0.59	0.37	37.18
ZnO- $\text{CeO}_2$ (Zn/Ce = 50:50)	17.85	32.84	0.54	0.35	35.21

### 2.2.3. Ultraviolet-visible spectroscopy (UV-vis)

DRUV-vis measurement was carried out by using Varian Cary 500 (Shimadzu) spectrophotometer. The spectra were recorded in the range of 200–800 nm wavelengths.

### 2.2.4. $\text{CO}_2$ -Temperature programmed desorption (TPD)

The TPD was carried out in a Micrometrics Chemisorb 2750 instrument (USA) equipped with a TCD detector. Prior to the analysis all the catalyst samples were purged with a He flow of 30 cc/min at 623 K temperature for 60 min to remove adsorbed water. The purged catalyst was cooled to ambient temperature.  $\text{CO}_2$  chemisorption was done passing 9.95% of  $\text{CO}_2$ /He mixture. The amounts of  $\text{CO}_2$  desorbed were evaluated by heating the sample up to 1273 K with ramp rate of 10 K/min in presence of He.

### 2.2.5. X-ray photoelectron spectroscopy (XPS)

The XPS analyses were carried out on a Kratos Ultra DLD spectrometer using monochromatic Al K $\alpha$  radiation (10 mA, 15 kV). All spectra were taken in the hybrid (combined electrostatic and magnetic lens) mode. Survey scans were conducted between 1200 eV and 0 binding energies with a step size of 1 eV, analyser pass energy 160 eV, and dwell time per step 100 ms, whereas scans over specific photoelectron regions were carried out at 20 eV pass energy and 200 ms dwell time. The specific photoelectron scans covered appropriate energy ranges, viz. 20 eV for O(1s) and C(1s), with 0.1 eV step size, 50 eV for Zn(2p) and 80 eV for Ce(3d), with 0.2 eV step size for the latter two. All spectra were referenced to the C(1s) line at binding energy 284.6 eV, characteristic of the ever-present adventitious carbon (C–C and C–H), and its exact peak position was obtained after Shirley background subtraction and decomposition of the C(1s) peak envelope using a Gaussian-Lorentzien (70%–30%) curve fit. All other photoelectron peaks were background-subtracted and curve-fit in the same manner. Quantification was carried out with the VISION software supplied. The relative sensitivity factors (RSF) applied here is inherent to this software and incorporate Wagner photoelectron cross-sections and analyser transmission correction.

**Table 4**

Quantitative XPS elemental analysis of Zinc-ceria mixed oxides.

Catalyst	Atom (%) Ce	Atom (%) Zn	Atom (%) O	Ce/Zn	O/(Ce + Zn)
ZnO-CeO <sub>2</sub> (Zn/Ce = 20:80)	18.2	9.6	53.4	1.89	1.92
ZnO-CeO <sub>2</sub> (Zn/Ce = 30:70)	21.1	9.6	51.6	2.19	1.68
ZnO-CeO <sub>2</sub> (Zn/Ce = 40:60)	17.4	12.3	50.8	1.41	1.71
ZnO-CeO <sub>2</sub> (Zn/Ce = 50:50)	16.5	12.0	51.3	1.375	1.8

**Table 5**

Binding energy and% of Peak area of O (1s) component of Zinc-ceria mixed oxides.

O (1s) Component →	a		b		c		d		
	Sample	B.E	% of Peak	Sample	B.E	% of Peak	Sample	B.E	% of Peak
CeO <sub>2</sub>		528.5	78.9		—	—	530.3	16.2	—
ZnO-CeO <sub>2</sub> (Zn/Ce = 20:80)		528.8	59.6		—	—	530.2	24.7	531.4
ZnO-CeO <sub>2</sub> (Zn/Ce = 30:70)		528.5	70.5		—	—	530.7	29.5	—
ZnO-CeO <sub>2</sub> (Zn/Ce = 40:60)		528.4	56.9	529.7	28.6	530.8	5.4	531.7	9.1
ZnO-CeO <sub>2</sub> (Zn/Ce = 50:50)		528.7	53.2	529.9	27.4	—	—	531.3	12.9
ZnO		—	—	529.8	70.9	—	—	531.2	29.2

**Table 6**

Catalytic activity data for oxidant free dehydrogenation reaction of benzyl alcohol over Zinc-ceria mixed oxide catalyst.

Catalyst	Conversion (%)	Selectivity (%)		STY (mol g <sup>-1</sup> cat h <sup>-1</sup> )	Mass balance (%)	Mears criteria *	C <sub>wp</sub> \$
		Benzaldehyde	Toluene				
CeO <sub>2</sub>	0.77	46.8	53.2	2.08	99.8	$4.34 \times 10^{-8}$	$3.65 \times 10^{-4}$
ZnO-CeO <sub>2</sub> (Zn/Ce = 20:80)	20.4	82.3	17.7	96.88	97.3	$2.02 \times 10^{-6}$	$1.75 \times 10^{-2}$
ZnO-CeO <sub>2</sub> (Zn/Ce = 30:70)	43.6	94.8	5.2	238.50	94.8	$4.97 \times 10^{-6}$	$4.19 \times 10^{-2}$
ZnO-CeO <sub>2</sub> (Zn/Ce = 40:60)	30.6	72.7	27.3	128.37	93.6	$2.68 \times 10^{-6}$	$6.70 \times 10^{-3}$
ZnO-CeO <sub>2</sub> (Zn/Ce = 50:50)	29.0	81.6	18.4	136.55	96.3	$2.85 \times 10^{-6}$	$8.15 \times 10^{-3}$

Reaction conditions: pretreatment temperature: 723 K; duration of pretreatment: 4 h; reaction temperature: 673 K; carrier gas ( $N_2$ ) flow: 30 ml/min, amount of catalyst: 0.5 g; particle size: 50  $\mu$ m; reaction time: 60 min; WHSV: 4000 h<sup>-1</sup>; Reynold number (Re):  $6.89 \times 10^{-4}$ ; Schmidt number ( $S_c$ ): 0.65; Sherwood number ( $S_h$ ): 2.01; \*calculated by Diwedi method; \$: Weisz criterion for internal diffusion.

### 2.2.6. Hydrogen temperature programmed reduction (H<sub>2</sub>-TPR)

The TPR measurements were carried out using Micromeritics Chemsorb 2750 apparatus. The pretreatment under high purity Argon flow was carried out at 573 K for half an hour. Then the catalyst was cooled to ambient temperature. Finally, furnace temperature was raised at 10 °C/min to 1273 K under 20 mL/min flow rate of H<sub>2</sub>/Ar mixture containing 10 vol.% of H<sub>2</sub>. The H<sub>2</sub> consumption was monitored by a thermal conductivity detector (TCD).

### 2.3. General procedure for alcohol dehydrogenation reaction

The catalytic experiments were carried out in a fixed bed reactor (1.5 cm id) at atmospheric pressure under N<sub>2</sub> flow. About 0.5 g of the catalyst was loaded and pretreatment was done in N<sub>2</sub> gas flow (purity 99.99%, 30 mL/min) at 723 K for 4 h. A thermocouple was inserted in the catalyst bed to measure the catalyst bed temperature. After pretreatment, the reactor was cooled to the desired reaction temperature and the reactant (benzyl alcohol) was fed at a flow rate of 3.0 mL h<sup>-1</sup> along with the N<sub>2</sub> gas flow at a rate of 30 mL/min to keep the WHSV at 8.56 h<sup>-1</sup>. The product was collected in an ice cold trap periodically for every 60 min and analyzed by a gas chromatograph (CIC, India) equipped with a flame ionization detector and SE-30 column. The oven temperature was kept at 483 K, with ramp rate 10 K/min whereas injector and detector temperature were kept at 503 K during the analysis.

The regeneration of the catalyst was done by treating the spent catalyst with O<sub>2</sub>/N<sub>2</sub> mixture (1:9 vol ratios) in the same flow as reaction condition at 673 K temperature. Then reactor was flushed with N<sub>2</sub> flow for one hour and feed mixture was introduced and product was collected and analyzed as described earlier.

In the case of dehydrogenation of primary alcohol substrates (ethanol, 1-Propanol, 1-butanol and 1-octanol) the reactor effluent was analyzed online for first three substrates and offline for

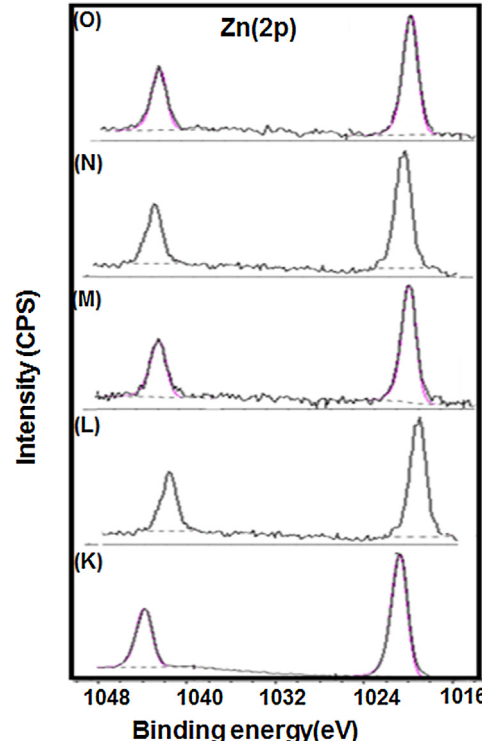


Fig. 7. Zn(2p) core level XPS spectra (K) ZnO, (L) ZnO-CeO<sub>2</sub> (Zn/Ce = 20/80), (M) ZnO-CeO<sub>2</sub> (Zn/Ce = 30:70), (N) ZnO-CeO<sub>2</sub> (Zn/Ce = 40/60) & (O) ZnO-CeO<sub>2</sub> (Zn/Ce = 50/50).

1-octanol. We used a gas chromatograph (CIC, India) equipped with a flame ionization detector and SE-30 column. All transfer lines

**Table 7**

Optimization of reaction temperature for oxidant free dehydrogenation reaction of benzyl alcohol over Zinc-ceria (Zn/Ce = 30/70) catalyst.

Catalyst	Reaction temperature K	Conversion (%)	Selectivity (%)		STY (mol g <sup>-1</sup> cat h <sup>-1</sup> )	Mass balance (%)
			Benzaldehyde	Toluene		
ZnO-CeO <sub>2</sub> (Zn/Ce = 30:70)	573	11.7	100	0	67.51	98.5
ZnO-CeO <sub>2</sub> (Zn/Ce = 30:70)	673	43.6	94.8	5.1	238.50	94.3
ZnO-CeO <sub>2</sub> (Zn/Ce = 30:70)	773	40.3	90.2	9.9	209.75	94.2

Reaction conditions: pretreatment temperature: 723 K; duration of pretreatment: 4 h; carrier gas (N<sub>2</sub>) flow: 30 ml/min, amount of catalyst: 0.5 g; particle size: 100 μm; reaction time: 60 min; WHSV: 4000 h<sup>-1</sup>.

**Table 8**

Optimization of pretreatment temperature for oxidant free dehydrogenation reaction of benzyl alcohol over Zinc-ceria (Zn/Ce = 30/70) catalyst.

Catalyst	Pretreatment Temperature (°C)	Conversion (%)	Selectivity (%)		STY (mol g <sup>-1</sup> cat h <sup>-1</sup> )	Mass balance (%)
			Benzaldehyde	Toluene		
ZnO-CeO <sub>2</sub> (Zn/Ce = 30:70)	350	24.3	73.7	26.2	103.34	>99
ZnO-CeO <sub>2</sub> (Zn/Ce = 30:70)	450	43.6	94.8	5.1	238.5	94.8
ZnO-CeO <sub>2</sub> (Zn/Ce = 30:70)	550	24.2	82.5	17.4	115.2	>99

Reaction conditions: duration of pretreatment: 4 h; reaction temperature: 673 K; carrier gas (N<sub>2</sub>) flow: 30 ml/min, amount of catalyst: 0.5 g; particle size: 100 μm; reaction time: 60 min; WHSV: 4000 h<sup>-1</sup>.

from the vaporizer to the reactor and gas chromatograph (GC) were heated to above 383 K to avoid condensation of the reactants and products. The oven temperature was kept at 383 K with ramp rate 5 K/min whereas injector and detector temperature were kept at 403 K during the online analysis. For 1-octanol dehydrogenation product, the G.C conditions were kept same as for benzyl alcohol.

Product i formation rate [C-mol kg cat<sup>-1</sup>, h<sup>-1</sup>] = (benzyl alcohol SV in C-mole kg cat<sup>-1</sup> h<sup>-1</sup>) × (C-moles in product i)/(total C – moles in products and un-reacted alcohol)

The absence of external limitation was confirmed by the Mears criterion [23] ( $-\dot{r}_A' p_b R \eta / k c_{AB}$ ) < 0.15 whose value was  $4.97 \times 10^{-6}$  for ZnO-CeO<sub>2</sub> (Zn/Ce = 30/70) catalyst. The absence of internal mass transfer was ascertained by means of the Weisz-Prater criterion ( $C_{WP} = -\dot{r}_A' p_c R^2 / D_e C_{AS}$ ) < 1 whose value was  $4.19 \times 10^{-2}$  in our case. The details of the calculations are provided in the supplementary material (Calculation S2).

### 3. Results and discussion

#### 3.1. Catalyst characterization

##### 3.1.1. BET S.A and porosity results

The adsorption/desorption isotherms and the corresponding pore size distributions of the studied catalysts are reported in Fig. 1. The isotherms can be observed in all cases characterized by the presence of a hysteresis loop indicating that the Zinc-ceria mixed oxide catalysts are mesoporous in nature [16]. The hysteresis loops which do not level off at relative pressures close to the saturation vapor pressure were reported for materials comprised of aggregates (loose assemblages) of plate like particles forming slit like pore [24]. The textural features of the samples have been investigated by BET surface area measurements and the results are reported in Table 1. Zinc-ceria mixed oxides changed the BET surface area slightly, but it did not affect the catalytic activity or the texture significantly [25]. The decrease in surface area after zinc incorporation has been observed. This may be due to pore blocking.

##### 3.1.2. X-ray diffraction (XRD)

Fig. 2 displays X-ray diffractions of the Zinc-ceria catalysts. It can be observed that diffraction peaks are attributable to the fluorite phase of ceria in all cases. XRD peaks are corresponding to ZnO crystal phases at (JCPDS card number 00-036-1451) 2θ values of 31.7, 34.4, 36.2 and 63.0 are observed for the Zinc-ceria catalysts with different ZnO contents. Fig. 2 shows that as increasing

the zinc loading, there is an increase in intensity of ZnO diffraction peaks observed in all cases. Table 2. Lists the crystalline size and the unit cell parameter of the Zinc-ceria catalysts. The Crystal sizes of both the Ceria and Zinc-ceria catalysts calculated by using Scherer's formula from the powder XRD data. The decrease in size of Zinc-ceria mixed oxides may be attributed to decrease in concentration of surface hydroxyls as low valent zinc substitutes the higher valent cerium in the lattice [26,27]

##### 3.1.3. UV-vis spectra

From the UV-vis study (Fig. 3.), it is found that in the pure CeO<sub>2</sub> and Zinc-ceria mixed oxides, the constant band at 280 nm can be ascribed to the intrinsic character of CeO<sub>2</sub> accordingly [28], while absorption edge at 413 nm in CeO<sub>2</sub> is blue shifted for Zinc-ceria mixed oxides, may indicate formation of Ce-O-Zn solid solution.

##### 3.1.4. Temperature programmed desorption (TPD) of CO<sub>2</sub>

The acid-base properties of zinc-ceria mixed oxide catalysts were measured by TPD using CO<sub>2</sub> as the acidic gas probe molecule Fig. 4. On metal oxide surface, basic sites are primarily associated to surface oxygen ions bonded to positively charge metal centers (Lewis acid sites) [29]. The strength of the basic sites has been estimated from the area under the corresponding TPD curve Fig. 5. At two desorption temperature ranges: for example, 323–523 K and 523–773 K. The basic sites at these temperature ranges have been designated as weak, medium and strong basic sites respectively [29,30]. As the reaction temperature was 673 K, so we chose the temperature till 773 K to observe the desorption of CO<sub>2</sub>. It is observed from CO<sub>2</sub>-TPD results that distribution of weak, medium and strong basic sites altered significantly by the incorporation of the zinc ion to the ceria matrix in different molar ratios. The total amount of desorbed carbon dioxide was highest for ZnO-CeO<sub>2</sub> (Zn/Ce = 50/50) catalyst as shown in Fig. 5 and Table S2.

##### 3.1.5. Cerium X-ray photoelectron spectroscopy (XPS)

The core level binding energies of CeO<sub>2</sub>, ZnO and ZnO-CeO<sub>2</sub> mixed oxides are displayed in Fig. 6 and 7. Which exhibits the characteristic binding energy peaks of Ce(3d), O(1s), and Zn(2p). All the binding energies are referenced to the adventitious elemental carbon (C1s) spectrum at 284.6 eV. As depicted in Table S1 (supporting information) the core level binding energy for Ce 3d<sub>5/2</sub> and Ce 3d<sub>3/2</sub> of the samples as well as quantitative analysis show some interesting features.

**Table 9**

Optimization of pretreatment time for oxidant free dehydrogenation reaction of benzyl alcohol over Zinc-ceria ( $Zn/Ce = 30/70$ ) catalyst.

Catalyst	Pretreatment Time (hours)	Conversion (%)	Selectivity (%)		STY ( $\text{mol g}^{-1} \text{cat h}^{-1}$ )	Mass Balance(%)
			Benzaldehyde	Toluene		
ZnO-CeO <sub>2</sub> ( $Zn/Ce = 30:70$ )	3 h	10.2	93.0	6.9	54.74	>99
ZnO-CeO <sub>2</sub> ( $Zn/Ce = 30:70$ )	4 h	43.6	94.8	5.1	238.5	94.8
ZnO-CeO <sub>2</sub> ( $Zn/Ce = 30:70$ )	5 h	11.64	89.02	10.98	59.79	>99

Reaction conditions: pretreatment temperature: 723 K; reaction temperature: 673 K; carrier gas ( $N_2$ ) flow: 30 ml/min, amount of catalyst: 0.5 g; particle size: 100  $\mu\text{m}$ ; reaction time: 60 min; WHSV: 4000  $\text{h}^{-1}$ .

**Table 10**

Time on stream study for the oxidant free dehydrogenation of benzyl alcohol over Zinc-ceria ( $Zn/Ce = 30/70$ ) catalyst.

Catalyst	Time on Stream (TOS) (min.)	Conversion (%)	Selectivity (%)		STY ( $\text{mol g}^{-1} \text{cat h}^{-1}$ )	Mass balance (%)
			Benzaldehyde	Toluene		
ZnO-CeO <sub>2</sub> ( $Zn/Ce = 30:70$ )	60	43.6	94.8	5.1	238.5	94.8
ZnO-CeO <sub>2</sub> ( $Zn/Ce = 30:70$ )	120	41.1	96.3	3.6	228.38	95.1
ZnO-CeO <sub>2</sub> ( $Zn/Ce = 30:70$ )	180	40.3	95.2	4.8	221.38	95.4

Reaction conditions: pretreatment temperature: 723 K; duration of pretreatment: 4 h; reaction temperature: 673 K; carrier gas ( $N_2$ ) flow: 30 ml/min, amount of catalyst: 0.5 g; particle size: 100  $\mu\text{m}$ ; reaction time: 60 min; WHSV: 4000  $\text{h}^{-1}$ .

The core level binding energies of Ce ( $3d_{5/2}$ ) and Ce ( $3d_{3/2}$ ) cerium compounds are known to exhibit rather complex features due to hybridization with ligand orbitals and fractional occupancy of the valence 4f orbital. Peaks around 881.4, 883.3, 887.9 and 897.3 eV are denoted as V,  $V^1$ ,  $V^{11}$ ,  $V^{111}$  (corresponding to Ce ( $3d_{5/2}$ ) states) whereas peaks at 901.7, 906.6 and 915.8 eV are denoted as  $U^1$ ,  $U^{11}$  and  $U^{111}$  (corresponding to Ce ( $3d_{3/2}$ ) states) respectively, as shown in Fig. 6. and Table S1,  $U^{11}/V^{11}$  doublet having the spin-orbit splitting of two states of 18.6 eV [31]. The  $U^{111}/V^{111}$  doublet is due to the primary photoemission from Ce(IV) $O_2$ , that is, Ce  $3d^9 4f^0 O 2p^6$  Ce (IV). The  $U^{11}/V^{11}$  doublets are shakedown features resulting from the transfer of one or two electrons from a filled O 2p orbital to an empty Ce 4f orbital, that is, Ce  $3d^9 4f^2 O 2p^4$  and Ce  $3d^9 4f^1 O 2p^5$  of Ce(IV) in the final states [32] whereas the  $U^1/V^1$  doublet has been assigned to photoemission from Ce cations, that is, Ce  $3d^9 4f^1 O 2p^6$  of Ce(III). The presence of the  $U^1$  peak in the spectrum indicates that the sample contains some oxygen vacancies and is in a partially reduced state, namely, Ce in +3 state. The Ce(3d) spectrum basically denotes a mixture of Ce<sup>3+</sup>/Ce<sup>4+</sup> oxidation states giving rise to a large number of peaks indicating that the surface of the sample is not fully oxidized [33]. The reduction is mainly due to the progressive elimination of surface hydroxyls and oxygen ions from the CeO<sub>2</sub> surface upon vacuum treatment. In the case of higher zinc loadings (Table S1) there is a shift in the binding energy of the peak due to Ce<sup>3+</sup> ( $U^1$ ) towards higher values which indicates interaction between zinc oxide and cerium oxide species, i.e. Ce-O-Zn bond formation.

As found in quantitative analysis (Tables 3 and 4), especially in ZnO-CeO<sub>2</sub> ( $Zn/Ce = 30/70$ ), the Ce<sup>3+</sup>/Ce<sup>4+</sup> ratio is minimum 0.43 that means among all cerium content of surface, 70% of total ceria ions are Ce<sup>4+</sup> and only 30% are Ce<sup>3+</sup>. This may be attributed to the replacement of Ce<sup>4+</sup> (ionic radii 101 pm) as well as Ce<sup>3+</sup> (ionic radii 115) by divalent Zn<sup>2+</sup> (ionic radii 88 pm).

### 3.1.6. Oxygen X-ray photoelectron spectroscopy

It is observed that O(1s) core level peaks as shown in Fig. 6. and Table 5 For the M-O-M' bonding where M and M' denote the metal with different electro negativities the O(1s) gives multiple peaks as reported in literature [34]. The peak at 528.6 eV can be assigned to ionic oxygen present in the mixed oxide. The peak at 529.8 eV can be assigned to either Ce<sub>2</sub>O<sub>3</sub> or ZnO as reported in literature. The O(1s) peak at 530.5 eV and 531.4 eV are mostly due to covalent oxygen species as also found in our earlier study [35]. Replacement of Ce<sup>4+</sup> or Ce<sup>3+</sup> by lower valent Zn<sup>2+</sup> increases the ionicity of Ce-O bond so

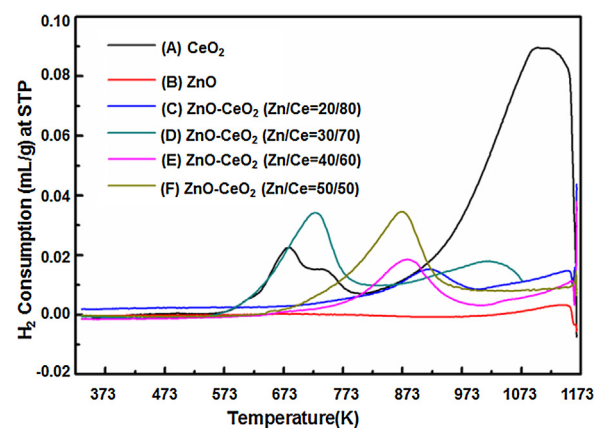


Fig. 8. H<sub>2</sub>-TPR of different catalysts (A) CeO<sub>2</sub>, (B) ZnO, (C) ZnO-CeO<sub>2</sub> ( $Zn/Ce = 20/80$ ), (D) ZnO-CeO<sub>2</sub> ( $Zn/Ce = 30/70$ ), (E) ZnO-CeO<sub>2</sub> ( $Zn/Ce = 40/60$ ) & (F) ZnO-CeO<sub>2</sub> ( $Zn/Ce = 50/50$ ).

maximum ionicity is also associated with ZnO-CeO<sub>2</sub> ( $Zn/Ce = 30/70$ ) mixed oxide [36]. When percentage of ZnO increases in CeO<sub>2</sub> lattice above than 30%, Ce<sup>3+</sup> fraction again increases which indicates replacement of Ce<sup>4+</sup> by Zn<sup>2+</sup> chiefly in higher zinc doping and the Ce-O bond become more covalent. (Table 5)

### 3.1.7. Zinc X-ray photoelectron spectroscopy

The XPS Zn(2p) Zinc-ceria mixed oxides is shown in Fig. 7. Quantitative XPS elemental analysis of Zinc-ceria mixed oxides are presented in Table 4. The XPS Zn(2p) spectrum of ZnO-CeO<sub>2</sub> mixed oxide shows the band chiefly around 1021 eV that may be Zn or ZnO [37–39]. To circumvent this difficulty, we have also measured the kinetic energy of the principal Auger peak ( $Zn L_3M_{45}M_{45}$ ) of zinc and we found a value of K.E. = 987.9 eV for the latter and this is more consistent with the ZnO (K.E.<sub>lit</sub> ~988 eV) rather than the metallic state (K.E.<sub>lit</sub> ~992 eV) [38]. It is found that Zn/Ce = 30/70 has less surface oxygen species compared to other Zn/Ce catalyst.

### 3.1.8. H<sub>2</sub>-temperature programmed reduction (TPR)

To know the reducibility of Ceria and Zinc-ceria mixed oxide catalysts of the hydrogen TPR was carried out and H<sub>2</sub> consumption vs Temperature plot is shown in Fig. 8. As reported in literature two reduction peaks appeared at 723 K and 1073 K temperature in the case of pure CeO<sub>2</sub>. These two peaks are mostly assigned to the surface capping oxygen ions and bulk oxygen [40]. Interestingly due

**Table 11**

Regeneration study for the oxidant free dehydrogenation of benzyl alcohol over Zinc-ceria ( $Zn/Ce = 30/70$ ) catalyst.

Regeneration No	Substrate	Conversion	Selectivity of BzOH	Selectivity of Toluene
Fresh run	Benzyl alcohol	43.6%	94.8%	5.2%
1		35.7%	70.56%	29.43%
2		29.34%	59.42%	40.57%

Reaction conditions: pretreatment temperature: 723 K; duration of pretreatment: 4 h; reaction temperature: 673 K; carrier gas ( $N_2$ ) flow: 30 ml/min, amount of catalyst: 0.5 g; particle size: 100  $\mu$ m; reaction time: 60 min; WHSV: 4000  $h^{-1}$ .

**Table 12**

Substrate variation study for the oxidant free dehydrogenation of different alcohol over Zinc-ceria ( $Zn/Ce = 30/70$ ) catalyst.

Reactant	Product 1(P1)	Product 2(P2)	Conversion (%)	Selectivity of P1(%)	Selectivity of P2(%)
1-propanol	Propanal	Propane			
			12.3	84.7	15.3
1-butanol	Butanal	Butane			
			19.9	68.9	31.0
Ethanol	Ethanal	Ethane			
			63.1	87.1	12.9
1-octanol	Octanal	Octane			
			14.4	99.3	0.7

Reaction conditions: pretreatment temperature: 723 K; duration of pretreatment: 4 h; reaction temperature: 673 K; carrier gas ( $N_2$ ) flow: 30 ml/min, amount of catalyst: 0.5 g; particle size: 100  $\mu$ m; reaction time: 60 min.

to doping by zinc in the mixed oxide becomes easily reducible at low temperature only. The  $Zn/Ce = 30/70$  sample has lowest reduction temperature in comparison with other Zinc-ceria mixed oxide catalysts. As observed from XPS and TPR results the  $Zn/Ce = 30/70$  had lowest  $Ce^{+3}/Ce^{4+}$  ratio i.e. more  $Ce^{4+}$  species so it can be easily reducible compared to other catalyst. (Table 4)

### 3.2. Catalytic activity results

#### 3.2.1. Effect of Ce-Zn ratio

The catalytic activities obtained over  $CeO_2$ ,  $ZnO$  and  $ZnO-CeO_2$  mixed oxide catalytic system towards benzyl alcohol dehydrogenation in vapor phase are shown in Table 6. It is found that  $CeO_2$  or  $ZnO$  catalyst system showed very little catalytic activity. However,  $ZnO-CeO_2$  mixed oxide systems shows enhanced catalytic activity. Among all,  $ZnO-CeO_2$  ( $Zn/Ce = 30/70$ ) catalyst showed best catalytic activity. From the XPS  $Ce(3d)$  spectra, it is found that  $ZnO-CeO_2$  ( $Zn/Ce = 30/70$ ) has least  $Ce^{+3}\%$  fraction and more ionic oxygen present in the catalyst surface. From the  $CO_2$ -TPD results it is found that  $ZnO-CeO_2$  ( $Zn/Ce = 30/70$ ) catalyst has more medium strength sites ranging temperature 673–723 K temperature. The TPR profile shows that  $ZnO-CeO_2$  ( $Zn/Ce = 30/70$ ) is highly reducible at lower temperature (673–723 K) compared to other catalysts. So it can be said that medium strength basic sites are responsible for higher catalytic activity,  $ZnO-CeO_2$  catalyst with  $Zn/Ce = 30/70$  ratio towards benzyl alcohol dehydrogenation reaction. The formation of toluene as a side product is observed after dehydrogenation reaction. The toluene formation was more for the catalyst which has more fractions of  $Ce^{3+}$  species i.e.  $ZnO-CeO_2$  catalyst with  $Zn/Ce = 40/60$  ratio.

#### 3.2.2. Effect of reaction temperature

Effect of reaction temperature on the catalytic activity was studied over  $ZnO-CeO_2$  catalyst ( $Zn/Ce = 30/70$ ) and shown in Table 7. At 573 K temperature, benzyl alcohol conversion is 12% and benzaldehyde selectivity is 100%. As temperature rises to 673 K, the best catalytic conversion 44% having 95% benzaldehyde selectivity is noticed. After further increase of reaction temperature to 773 K, catalytic conversion was decreases to 40%. As the reaction temperature rises, benzaldehyde selectivity was decreased and toluene selectivity was increased. As described earlier the basic sites with medium strength having  $CO_2$  desorption temperature at 673 K are responsible for abstracting the hydrogen atom from benzyl alcohol during the initial step of the reaction.

#### 3.2.3. Effect of pretreatment temperature and pretreatment time

The effect of pretreatment temperature and pretreatment time on benzyl alcohol conversion and benzaldehyde selectivity over  $ZnO-CeO_2$  ( $Zn/Ce = 30/70$ ) catalysts are shown in Tables 8 and 9. Respectively. At 723 K pretreatment temperature and 4 h pretreatment time,  $ZnO-CeO_2$  ( $Zn/Ce = 30/70$ ) catalyst shows optimum performance. It should be also noticed that both at lower and higher pretreatment temperatures, conversion of benzyl alcohol is almost equal but toluene selectivity increased with the expense of benzaldehyde selectivity.

#### 3.2.4. Time on stream (TOS) study

In order to find out whether the catalyst was deactivated in long run the catalyst activity of  $ZnO-CeO_2$  ( $Zn/Ce = 30/70$ ) catalyst was evaluated for till 3 h time on stream as shown in Table 10. On increasing time on stream up to six hours, benzyl alcohol conversion, benzaldehyde selectivity and toluene selectivity varied in

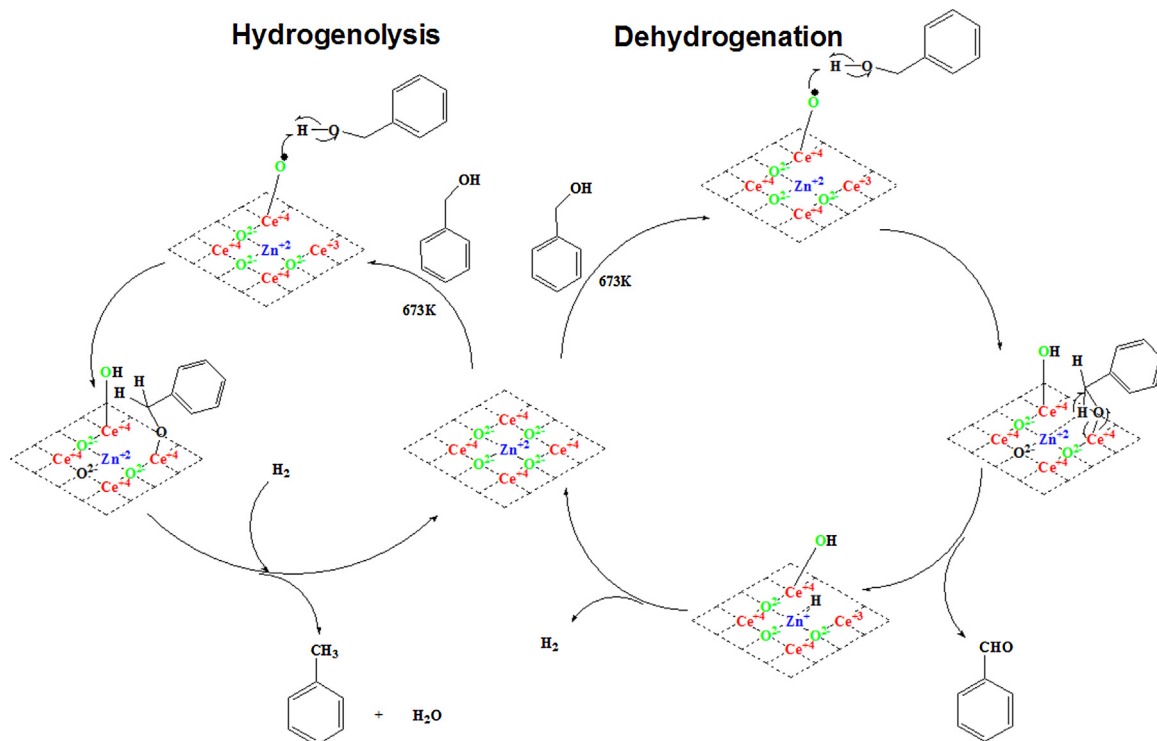


**Fig. 9.** The proposed reaction mechanism of benzyl alcohol transformation over ZnO-CeO<sub>2</sub> catalyst surface.

small amount (supporting information; Fig. S1). Overall, it can be said that the zinc containing ceria catalyst system showed better activity and slower deactivation. Previously, C.Yu. et al. have shown that zinc addition in catalytic system enhances the dehydrogenation activity of propane and retard the coke formation [41]. Similarly, we found that ZnO-CeO<sub>2</sub> (Zn/Ce = 30/70) is also most active towards the benzyl alcohol dehydrogenation reaction as well as it has least deactivation.

### 3.2.5. Effect of catalyst regeneration

The spent catalyst was regenerated using a mixture of O<sub>2</sub> and N<sub>2</sub> gas (1:9 vol ratios) at 723 K temperature for two hours (Table 11). It is observed that both the benzyl alcohol conversion and benzaldehyde selectivity decreased in recycling whereas toluene selectivity was increased.

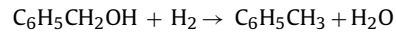
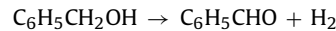
### 3.2.6. Substrate variation

After obtaining satisfactory result we have carried out the oxidant free dehydrogenation of various primary alcohols e.g. ethanol, 1-propanol, 1-butanol and 1-octanol. Interestingly we found high selectivity towards dehydrogenated products as depicted in Table 12. In the case of ethanol, 1-propanol, 1-butanol and 1-octanol along with the corresponding aldehydes saturate hydrocarbons i.e. ethane, propane, butane and octane were also obtained which evidenced in-situ generation of hydrogen.

## 4. Proposed mechanism

From the experimental results and literature reports it can be said that initially hydrogen atom is abstracted by oxygen radical species from hydroxyl group of benzyl alcohol and oxo-metal species formed. Further, Ce<sup>4+</sup> species converted to Ce<sup>3+</sup> species. Then zinc site cleaved the C-H bond of Ph-CH<sub>2</sub> group formation of benzaldehyde occurs by liberation of hydrogen. Later hydrogenol-

ysis of benzyl alcohol takes place in presence of hydrogen resulting formation of toluene occurs (Fig. 9).



In the case Zn/Ce (30/70 ratio) catalyst, the percentage of ionicity is more compared to other catalysts in the series. The CO<sub>2</sub>-TPD study shows that medium strength basic sites (in the desorption temperature 673–773 K) are highly populated for the catalyst Zn/Ce ratio (30/70). In general benzaldehyde after hydrogenation gives benzyl alcohol but surprisingly we got toluene due to hydrogenolysis of benzyl alcohol. The selectivity of toluene is found to increase with increasing surface coverage of Ce<sup>3+</sup>. So, similarly ethane, propane, butane and octane were obtained due to hydrogenolysis of ethanol, 1-propanol, 1-butanol and 1-octanol respectively. We have measured the XPS of the used catalyst ZnO-CeO<sub>2</sub> (Zn/Ce = 30/70). The quantitative analysis shows Ce<sup>3+</sup>/Ce<sup>4+</sup> ratio has been increased which indicates that catalyst was reduced during reaction (supporting information Table S1, S2, S3, S4 and Fig. S2). The TPR profile of fresh and used ZnO-CeO<sub>2</sub> (Zn/Ce = 30/70) catalyst showed that peak due to ceria reduction shifted to higher temperature (supporting information; Fig. S3). It implies that used catalyst was difficult to reduce. The UV-vis spectra of fresh and used ZnO-CeO<sub>2</sub> catalyst (Zn/Ce = 30/70) are recorded. The absorption edges of the mixed oxides (412 nm for ZnO-CeO<sub>2</sub> (Zn/Ce = 30/70) fresh catalyst and 438 nm benzyl alcohol adsorbed ZnO-CeO<sub>2</sub> (Zn/Ce = 30/70) shifts to visible range remarkably. The band gap of the samples is calculated by using the formula E<sub>g</sub> (eV) = 1240/λ<sub>g</sub> (nm), where λ<sub>g</sub> stands for the wavelength value corresponding to the intersection point of the vertical and horizontal part of the spectra, the red shift of absorption edges and narrowing of band gaps (3.00 eV for ZnO-CeO<sub>2</sub> (Zn/Ce = 30/70) fresh catalyst and 2.83 eV for benzyl alcohol adsorbed ZnO-CeO<sub>2</sub> (Zn/Ce = 30/70) observed in the UV-vis spectra [42]. IR spectra of used catalyst showed the adsorbed benzyl

alcohol and benzaldehyde species present in the catalyst surface (supporting information; Fig. S4). From the FTIR spectra of used ZnO-CeO<sub>2</sub> (Zn/Ce = 30/70) catalyst the band appeared at 1029 cm<sup>-1</sup>, 1425 cm<sup>-1</sup>, 1639 cm<sup>-1</sup>, 2921 cm<sup>-1</sup>, 3165 cm<sup>-1</sup> which correspond to side chain hydroxyl of benzyl alcohol, C=C stretching of benzene ring, C-H stretching of methylene group in toluene, C=O stretching of benzaldehyde and O-H stretching of benzyl alcohol respectively (Fig. S5) [43]. Based on this observation the proposed mechanism is justified.

## 5. Conclusions

In a nutshell, Zinc-ceria mixed oxide catalysts was developed for the dehydrogenation of benzyl alcohol in oxidant free condition. There is no phase separation of zinc oxide while incorporated in ceria matrix as observed from XRD study for Zn/Ce (30/70). The populations of medium strength basic sites are more for the catalyst having Zn/Ce in the ratio of 30/70 as found from CO<sub>2</sub>-TPD studies. Eventually XPS results reveal that Ce<sup>3+</sup>/Ce<sup>4+</sup> ratio was least for Zinc-ceria mixed oxide catalyst having Zn/Ce = 30/70 ratio. Also the contribution of ionic oxygen was more for the same catalyst. The catalyst having more oxygen vacancy, more ionicity renders best activity for formation of benzaldehyde. The formation of toluene, ethane, propane, butane and octane as by product due to hydrogenolysis is an interesting observation in the present study.

## Acknowledgment

EN would like to acknowledge DST for junior research fellowship. SH acknowledges UGC for research fellowship. RK acknowledges ISM for providing research fellowship. BC would like to acknowledge Science and Engineering Research Board (SERB), DST, Govt of India for funding under major project (SB/S1/PC-10/2012). BC would also like to acknowledge Prof. Juan Bravo-suarez, University of Kansas, USA to help in micro-kinetic analysis. Authors would like to acknowledge Dr. Swami Prakash for helping in XPS measurement.

## Appendix A. Supplementary data

Supplementary data associated with this article can be found, in the online version, at <http://dx.doi.org/10.1016/j.apcata.2016.05.003>.

## References

- [1] Sabatier, Mailhe, Ann. Chim. Phys. 20 (1910) 289–341.
- [2] Balandin, Tetenyi, Russ. J. Phys. Chem. 35 (1961) 28.
- [3] Ghosh, Bakshi, J. Indian Chem. Soc. 3 (1926) 415.
- [4] T. Mitsudome, Y. Mikami, H. Funai, T. Mizugaki, K. Jitsukawa, K. Kaneda, Angew. Chem. 120 (2008) 144–147;
- T. Mitsudome, Y. Mikami, H. Funai, T. Mizugaki, K. Jitsukawa, K. Kaneda, Angew. Chem. Int. Ed. 47 (2008) 138–141.
- [5] T. Mitsudome, Y. Mikami, K. Ebata, T. Mizugaki, K. Jitsukawa, K. Kaneda, Chem. Commun. 3 (2008) 4804–4806.
- [6] K. Shimizu, K. Sugino, K. Sawabe, A. Satsuma, Chem. Eur. J. 15 (2009) 2341–2351.
- [7] V.R. choudhary, P.A. Chaudhari, V.S. Narkhede, Catal. Commun. 4 (2003) 171–175.
- [8] G. Centi, F. Cavani, F. Trifiro, Selective Oxidation by Heterogeneous Catalysis, Kluwer Academic/Plenum Publishers, New York, 2001.
- [9] W. Fang, Q. Zhang, J. Chen, W. Deng, Y. Wang, Chem. Commun. 46 (2010) 1547–1549.
- [10] S. Meenakshisundaram, E. Nowicka, P.J. Miedziak, G.L. Brett, R.L. Jenkins, N. Dimitratos, S.H. Taylor, D.W. Knight, D. Bethell, G.J. Hutchings, Faraday Discuss. 145 (2010) 341–356.
- [11] M.T. Musser, in: M. Bohnet (Ed.), Ullmann's Encyclopedia of Industrial Chemistry, 10, 6th edn., VCH, Weinheim, 2003, p. 284.
- [12] S. Mandal, C. Santra, K.K. Bando, O.O. James, S. Maity, D. Mehta, B. Chowdhury, J. Mol. Catal. A 378 (2013) 47–56.
- [13] X. Wang, J.A. Rodriguez, J.C. Hanson, D. Gamarra, A. Martinez-Arias, M.F. Garcia, J. Phys. Chem. B 110 (2006) 428–434.
- [14] D. Gamarra, C. Belver, M. Fernandez-Garcia, A. Martinez-Arias, J. Am. Chem. Soc. 129 (2007) 12064–12065.
- [15] S.K. Pahari, P. Pal, A. Sinhamahapatra, A. Saha, C. Santra, S.C. Ghosh, B. Chowdhury, A.B. Panda, RSC Adv. 5 (2015) 45144–45151.
- [16] G. Postole, B. Chowdhury, B. Karmakar, K. Pinki, J. Banerji, A. Auoux, J. Catal. 269 (2010) 110–121.
- [17] Y. Zhang, S. Andersson, M. Muhammed, Appl. Catal. B 6 (1995) 325–337.
- [18] P. Fornasiero, G. Baldacci, R. Di Monte, J. Kaspar, V. Sergio, G. Gubitoso, A. Ferrero, M. Graziani, J. Catal. 164 (1996) 173–183.
- [19] A.E.C. Palmqvist, E.M. Johansson, S.G. Järas, M. Muhammed, Catal. Lett. 56 (1998) 69–75.
- [20] H. Imai, K. Nakamura, React. Kinet. Catal. Lett. 43 (1991) 355–359.
- [21] Y. He, B. Yang, G. Cheng, Catal. Today 98 (2004) 595–600;
- Y. He, X. Yu, T. Li, L. Yan, B. Yang, Powder Technol. 166 (2006) 72–76.
- [22] B.G. Mishra, G.R. Rao, J. Mol. Catal. A 243 (2006) 204–213.
- [23] J.J. Bravo-Suárez, B. Subramaniam, R.V. Chaudharia, Appl. Catal. A Gen. 455 (2013) 234–246.
- [24] M. Kruck, M. Jaroniec, Chem. Mater. 13 (2001) 3169–3183.
- [25] L.F. Nacimento, R.F. Martins, R.F. Silva, O.A. Serra, J. Environ. Sci. 26 (2014) 694–701.
- [26] S. Tsunekawa, K. Ishikawa, Z.Q. Li, Y. Kawazoe, A. Kasuya, Phys. Rev. Lett. 85 (2000) 3440–3443.
- [27] N. Sutradhar, A. Sinhamahapatra, S. Pahari, M. Jayachandran, B. Subramanian, H.C. Bajaj, A.B. Panda, J. Phys. Chem. C 115 (2011) 7628–7637.
- [28] C.J. Tighe, R.Q. Cabrera, R.I. Gruar, J.A. Darr, Ind. Eng. Chem. Res. 52 (2013) 5522–5528.
- [29] C. Santra, S. Rahman, S. Bojja, O.O. James, D. Sen, S. Maity, A.K. Mohanty, S. Mazumder, B. Chowdhury, Catal. Sci. Technol. 3 (2013) 360–370.
- [30] J. Guzman, S. Carrettin, A. Corma, J. Am. Chem. Soc. 127 (2005) 3286–3287.
- [31] W. Fang, Q. Zhang, J. Chen, W. Deng, Y. Wang, Chem. Commun. 46 (2010) 1547.
- [32] V. Shapovalov, H. Metiu, J. Catal. 245 (2007) 205–214.
- [33] A.K. Sinha, K. Suzuki, J. Phys. Chem. B 109 (2005) 1708–1714.
- [34] B.M. Reddy, G. Thrimurthulu, L. Katta, Y. Yamada, S.E. Park, J. Phys. Chem. C 113 (2009) 15882–15890.
- [35] B.R. Strommeier, D.M. Hercules, J. Catal. 86 (1984) 266–279;
- Q. Xie, Y. Zhao, H. Guo, A. Lu, X. Zhang, L. Wang, M.S. Chen, D.L. Peng, ACS Appl. Mater. Interfaces 6 (2014) 421–428.
- [36] D.O. Scanlon, A. Walsh, B.J. Morgan, M. Nolan, J. Fearon, G.W. Watson, J. Phys. Chem. C 111 (2007) 7971–7979;
- J. Phys. Condens. Matter 18 (2006) R667–R704;
- Z. Yang, Q. Wang, S. Wei, Phys. Chem. Chem. Phys. 13 (2011) 9363–9373;
- Z. Yang, B. He, Z. Lu, K. Hermansson, J. Phys. Chem. C 114 (2010) 4486–4494.
- [37] Z.L. Long, Y.C. Zhou, L. Xial, Appl. Surf. Sci. 218 (2003) 124–137.
- [38] Q. Xie, Y. Zhao, H. Guo, A. Lu, X. Zhang, L. Wang, M.-S. Chen, D.-L. Peng, ACS Appl. Mater. Interfaces 6 (2014) 421–428.
- [39] S. Anandan, M. Miyauchi, Phys. Chem. Chem. Phys. 13 (2011) 14937–14945.
- [40] S. Mandal, K.K. Bando, C. Santra, S. Maity, O.O. James, D. Mehta, B. Chowdhury, Appl. Catal. A 452 (2013) 94–104.
- [41] C. Yu, H. Xu, Q. Ge, W. Li, J. Mol. Catal. A Chem. 266 (2007) 80–87.
- [42] N. Sinha, G. Ray, S. Bhandari, S. Godara, B. Kumar, Ceram. Int. 40 (2014) 12337–12342.
- [43] R.M. Silverstein, F.X. Webster, Spectroscopic Identification of Organic Compounds, 6th edn., Wiley & Sons, 1998.